

Optical nonreciprocity induced by quantum squeezing in temperature sensitive optomechanical systems

Jun-Cong Zheng, Xiao-Wei Zheng, Xin-Lei Hei, Yi-Fan Qiao, Xiao-Yu Yao, Xue-Feng Pan, Yu-Meng Ren, Xiao-Wen Huo and Peng-Bo Li*

Ministry of Education Key Laboratory for Nonequilibrium Synthesis and Modulation of Condensed Matter, Shaanxi Province Key Laboratory of Quantum Information and Quantum Optoelectronic Devices, School of Physics, Xi'an Jiaotong University, Xi'an 710049, China

E-mail: lipengbo@mail.xjtu.edu.cn

Keywords: nonreciprocal, quantum squeezing, optomechanical systems

Abstract. We investigate single-photon transmission and the statistical properties of photon correlations in $\chi^{(2)}$ microring optomechanical systems, where optical nonreciprocity is induced by directional quantum squeezing. Due to the presence of thermal phonons in the mechanical resonator, the system is highly sensitive to temperature changes. Our numerical simulations show that as the thermal phonons vary from 0 to 10, the isolation ratio of single-photon transmission decreases from 22.2 dB to 1.1 dB (or from -23 dB to -3.3 dB). Additionally, the statistical properties of photon correlations transition from exhibiting a strong bunching effect to a weak bunching effect. Moreover, the parametric amplification component enhances the device's temperature response, distinguishing it from other similar nonreciprocal devices. Our protocol suggests a potential application for nonreciprocal setups in precise temperature measurement at ultralow temperatures, thereby enriching quantum networks and quantum information processing.

1. Introduction

Optomechanical systems, which explore the interaction between electromagnetic radiation and nanomechanical elements, have advanced significantly in recent years [1–7]. Based on the radiation modes and vibrational degrees of freedom, optomechanical systems can be categorized into different types of setups, including suspended micropillars [8], suspended membranes [9], optical microsphere resonators [10], and near-field coupled nanomechanical oscillators [11]. The last type of setup is commonly found in microring optomechanical systems, which benefit from directional evanescent coupling [12–18]. In these microring optomechanical systems, there are both clockwise (CW) and counterclockwise (CCW) modes in the optical resonator, making them

suitable for achieving optical nonreciprocity by inducing the splitting of degenerate modes [19–24]. Compared to traditional purely optical nonreciprocal devices [25–31], these optomechanical systems can link nonreciprocal effects to ambient temperature, offering potential applications in temperature measurement at ultralow temperatures [24]. However, weak optomechanical coupling remains a challenge for achieving precise measurements, and strengthening the optomechanical coupling in these nonreciprocal systems is a key focus for future research.

Quantum squeezing [32–35], an important resource in the field of quantum information, is typically generated through fully quantum degenerate parametric amplifiers (DPAs) [36, 37] or semiclassical DPAs [38–40]. It is often applied to manipulate zero-point motion, enabling the realization of ultrasensitive sensing of force and motion [41–49]. Recent research has focused on quantum squeezing in a $\chi^{(2)}$ resonator mode, achieving exponentially enhanced optomechanical coupling [50]. Other studies have realized optical nonreciprocity through directional quantum squeezing in $\chi^{(2)}$ microring optical systems [51, 52]. Building on these contributions, precise temperature measurement using nonreciprocal devices, as mentioned earlier, becomes feasible.

In this work, we simultaneously achieved optical nonreciprocity and enhanced optomechanical coupling, both induced by quantum squeezing in a microring optomechanical system. Specifically, we incorporate an additional mechanical resonator coupled to the optical resonators, building on the configuration in Refs. [51, 52]. In this case, the transmission of incident photons is influenced by thermal phonons. Our numerical simulations show that as the temperature changes, the effectiveness of single-photon nonreciprocal transmission diminishes, and the statistical properties of photons evolve from exhibiting a strong bunching effect to a weak bunching effect. Additionally, quantum squeezing enhances the optomechanical coupling between the optical resonator and the mechanical resonator. As shown in Fig. 1, we placed the oscillator in three different regions, including regions with reinforced optomechanical coupling and regions where the coupling remains invariant. The results indicate that the directional parametric amplification component (with the mechanical oscillator placed in Area I or Area III) has a more pronounced effect on photon transmission. In conclusion, our method provides a platform for achieving optical nonreciprocity in temperature-sensitive optomechanical systems. This approach could potentially be extended to acoustic modes, where nonlinear acoustic devices can be realized by coupling to a two-level system [53, 54]. Acoustic diodes, which are widely used in phonon-based quantum information processing [55–59], could benefit from such advancements.

This work is structured as follows: In Section 2, we introduce the model of temperature-sensitive optomechanical systems and present the corresponding Hamiltonian. Moving on to Sections 3 and 4, we show the response of single-photon nonreciprocal transport and the statistical properties of correlated photons to temperature changes, respectively. Section 5 is dedicated to a discussion on experimental feasibility, and finally, Section 6 provides a summary of the findings.

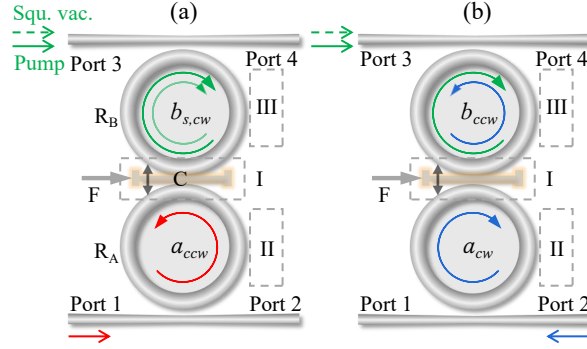


Figure 1. Schematic diagram illustrating the generation of ambient temperature-sensitive nonreciprocal single-photon isolation and nonreciprocal photon correlations. Two microring resonators, named R_A and R_B , are coupled to a lower bus waveguide (at a rate κ_a) and an upper drop waveguide (at a rate κ_b), respectively. The mechanical nanostring oscillator C (driven by a force F) is placed at three different locations: areas I, II, and III. A coherent pump field and a broadband squeezed-vacuum field are input from port 3, with the squeezed CW mode in R_B denoted as $b_{s,cw}$. (a) A probe field input from port 1 excites a CCW mode a_{ccw} in R_A , which interacts with the oscillator C and the mode $b_{s,cw}$, respectively. (b) A probe field input from port 2 excites a CW mode a_{cw} in R_A , which interacts with the oscillator C and the mode b_{ccw} , respectively.

2. Physical model

We aim to correlate the nonreciprocal effect induced by quantum squeezing with ambient temperature in a microring optomechanical system. By leveraging the strong optomechanical coupling generated through parametric amplification [50], this setup shows potential for applying nonreciprocal systems in precise temperature measurements. The schematic of the proposed system is illustrated in Fig. 1. Two microring resonators, R_A and R_B , with $\chi^{(2)}$ nonlinearity, are made of high-quality thin film and interact with each other via the optical evanescent field with coupling strength g_0 . The mechanical resonator C is placed in area I, located in the middle of the gap between R_A and R_B , and is simultaneously optomechanically coupled to these two optical resonators with coupling strength j_0 but with opposite signs [24, 60] (refer to Appendix A for details). In this case, the semi-classical optomechanical Hamiltonian of the mechanical mode is expressed as (setting $\hbar = 1$)

$$H_m^I = \frac{1}{2}\omega_m(q^2 + p^2) - \sum_{\xi=cw,ccw} j_0(a_\xi^\dagger a_\xi - b_\xi^\dagger b_\xi)q, \quad (1)$$

where a_ξ , b_ξ , a_ξ^\dagger , and b_ξ^\dagger ($\xi = cw, ccw$) denote the annihilation and creation operators of optical modes with frequencies ω_a and ω_b , respectively, q and p represent the dimensionless displacement and momentum operators of the mechanical resonator with frequency ω_m . These operators for the mechanical resonator can be expressed in terms of phonon creation and annihilation operators as $q = (c^\dagger + c)/\sqrt{2}$ and $p = i(c^\dagger - c)/\sqrt{2}$.

Consequently, the fully quantized Hamiltonian is given by:

$$\mathcal{H}_m^I = \omega_m c^\dagger c - \sum_{\xi=cw,ccw} J_0 (a_\xi^\dagger a_\xi - b_\xi^\dagger b_\xi) (c^\dagger + c), \quad (2)$$

where $J_0 = j_0/\sqrt{2}$, the constant term $\omega_m/2$ can be nullified by selecting an appropriate gauge. Additionally, the resonator C , positioned in areas II and III, interacts with the single resonators R_A and R_B , respectively. The corresponding Hamiltonians are expressed as:

$$\mathcal{H}_m^{II} = \omega_m c^\dagger c - \sum_{\xi=cw,ccw} J_0 a_\xi^\dagger a_\xi (c^\dagger + c), \quad (3)$$

$$\mathcal{H}_m^{III} = \omega_m c^\dagger c - \sum_{\xi=cw,ccw} J_0 b_\xi^\dagger b_\xi (c^\dagger + c). \quad (4)$$

Now, we discuss how the configuration works. We consider that C is initially placed in area I (corresponding to the Hamiltonian \mathcal{H}_m^I). A continuous-wave coherent laser field with frequency ω_s and strength Ω , pumped from port 3, squeezes the CW mode b_{cw} in R_B into $b_{s,cw}$ under the two-mode phase-matching condition [51, 52, 61], while remaining decoupled from the CCW mode b_{ccw} . As shown in Fig. 1(a), a weak probe field with frequency ω_p and amplitude ε , input from port 1, excites the CCW mode a_{ccw} in R_A . Due to the pump field, mode a_{ccw} interacts with the squeezed mode $b_{s,cw}$ at an effective rate g_s . Regarding the optomechanical coupling, the oscillator C interacts with the squeezed mode $b_{s,cw}$ at an effective rate J_s , and with the mode a_{ccw} at the unmodulated rate J_0 . It is important to note that we neglect the coupling of oscillator C with the CCW mode in R_B and the CW mode in R_A in the following discussion, as their effects on photon transmission in the system are negligible (refer to Appendix C for details).

In the rotating reference frame defined by the unitary operator $R(t) = \exp[i\omega_s(a_{ccw}^\dagger a_{ccw} + b_{cw}^\dagger b_{cw})t/2]$, the Hamiltonian of the entire system for the case of a probe field input from port 1 is expressed as:

$$\begin{aligned} \mathcal{H}_1 &= \mathcal{H}_0 + \mathcal{H}_{int} + \mathcal{H}_p + \mathcal{H}_s + \mathcal{H}_f, \\ \mathcal{H}_0 &= \Delta_s^a a_{ccw}^\dagger a_{ccw} + \Delta_s^b b_{cw}^\dagger b_{cw} + \omega_m c^\dagger c, \\ \mathcal{H}_{int} &= g_0 (a_{ccw}^\dagger b_{cw} + a_{ccw} b_{cw}^\dagger) - J_0 (a_{ccw}^\dagger a_{ccw} - b_{cw}^\dagger b_{cw}) (c^\dagger + c), \\ \mathcal{H}_p &= i\sqrt{\kappa_{ex1}} (\varepsilon a_{ccw}^\dagger e^{-i\Delta_p t} - \varepsilon^* a_{ccw} e^{i\Delta_p t}), \\ \mathcal{H}_s &= \frac{\Omega}{2} (b_{cw}^{\dagger 2} + b_{cw}^2), \\ \mathcal{H}_f &= F(c^\dagger + c), \end{aligned} \quad (5)$$

where \mathcal{H}_0 represents the free Hamiltonian for the microring resonators and the mechanical oscillator. \mathcal{H}_{int} denotes the interaction Hamiltonian, with the first term representing pure photon exchange and the second term reflecting the exchange between photons and phonons. \mathcal{H}_p and \mathcal{H}_s denote the Hamiltonians of the probe field and the

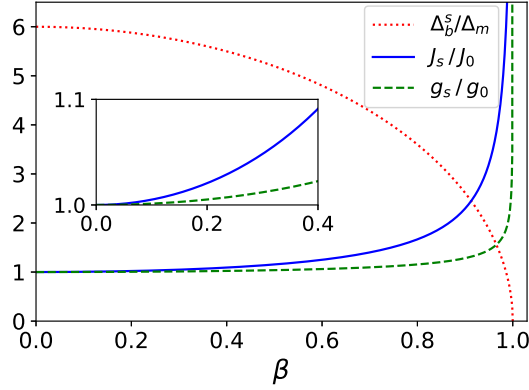


Figure 2. The squeezing parameters, including the effective squeezed mode detuning Δ_b^s (red dotted line), the effective coupling rates J_s (blue solid line), and g_s (green dashed line), are shown as functions of the pump ratio $\beta \in [0, 1)$. Other parameters are set as $\Delta_s^b = 6\Delta_m$ and $\Delta_p = 0$.

squeezing pump field, respectively. Additionally, we introduce a constant Hamiltonian \mathcal{H}_f for the mechanical mode to counteract the force induced by the parametric amplification (see below). The detunings are $\Delta_s^{a/b} = \omega_{a/b} - \omega_s/2$, $\Delta_p = \omega_p - \omega_s/2$, and κ_{ex1} is the external decay rate of resonator R_A .

To calculate the scattering of incident photons from port 1, we can transform the Hamiltonian \mathcal{H}_1 into the squeezing picture. By applying the Bogoliubov squeezing transformation $b_s = \cosh(r_s)b + \sinh(r_s)b^\dagger$ [36, 50], with the squeezing parameter $r_s = \frac{1}{4}\ln[(1 + \beta)/(1 - \beta)]$, where $\beta = \Omega/\Delta_s^b$ is the pump ratio, the Hamiltonian in the frame rotating at the frequency of Δ_p becomes (refer to Appendix B for details):

$$\begin{aligned} \mathcal{H}_1^s = & \Delta_a a_{ccw}^\dagger a_{ccw} + i\sqrt{\kappa_{ex1}}(\varepsilon a_{ccw}^\dagger - \varepsilon^* a_{ccw}) + \Delta_m c^\dagger c \\ & + \Delta_b^s b_{s,cw}^\dagger b_{s,cw} + g_s(a_{ccw}^\dagger b_{s,cw} + a_{ccw} b_{s,cw}^\dagger) \\ & - (J_0 a_{ccw}^\dagger a_{ccw} - J_s b_{s,cw}^\dagger b_{s,cw})(c^\dagger + c). \end{aligned} \quad (6)$$

We have neglected the parametric interaction [50] and the counter-rotating terms under the rotating-wave approximation ($g_0 \sinh(r_s) \ll \Delta_s^a + \Delta_s^b \sqrt{1 - \beta^2}$). Additionally, the induced force applied to the mechanical oscillator is canceled by the additional force $F = -J_0 \sinh^2(r_s)$, which remains constant once the squeezing parameter is fixed. We define $\Delta_a = \Delta_s^a - \Delta_p$, $\Delta_b^s = \Delta_s^{bs} - \Delta_p$, $\Delta_s^{bs} = \Delta_s^b \sqrt{1 - \beta^2}$, $\Delta_m = \omega_m - \Delta_p$, and $g_s = g_0 \cosh(r_s)$, $J_s = J_0 \cosh(2r_s)$. Here, Δ_b^s and g_s , J_s are the effective squeezed mode detuning and the effective couplings, respectively, adjusted by the squeezing pump field.

To quantify the influence of the squeezing pump field \mathcal{H}_s , we plot the detuning Δ_b^s/Δ_m and the coupling ratios J_s/J_0 and g_s/g_0 versus the pump ratio β in Fig.2. Initially, at $\beta = 0$, the parameters correspond to the normal mode situation. As β increases, Δ_b^s/Δ_m exhibits a parabolic decrease, eventually approaching 0 near $\beta = 1$. For the coupling ratios, before $\beta = 0.9$, J_s/J_0 and g_s/g_0 increase gradually, with g_s/g_0 increasing slightly more slowly than J_s/J_0 , indicating that the

coupling with the mechanical nanostring oscillator is more responsive to the squeezing pump. Additionally, the simulation shows that both the squeezed detuning and the coupling react dramatically (i.e., exponentially decreasing and exponentially increasing, respectively) as the pump ratio approaches $\beta = 1$. From a physical perspective, the enhancement in coupling strength arises from a single-photon state in the squeezed mode, which corresponds to an exponentially increasing number of photons in the R_B as the squeezing strength increases. Consequently, the radiation pressure exerted by a single squeezed photon on both the R_A and the mechanical resonator also increases, thereby strengthening the coupling with the squeezed cavity mode. Furthermore, the optical coupling grows much more slowly than the optomechanical coupling, as the former's coupling strength is primarily determined by the amplitude of the optical field and does not directly depend on changes in photon number. In contrast, the latter's coupling strength is directly dependent on the photon number within the squeezed cavity.

In Fig.1(b), the weak probe field input from port 2 excites the CW mode a_{cw} , which interacts with the CCW mode b_{ccw} in R_B at a rate of g_0 . Regarding the optomechanical coupling, the oscillator C interacts with both mode a_{cw} and mode b_{ccw} at a rate of J_0 . we neglect the coupling of oscillator C with the CW mode in R_B and the CCW mode in R_A in the following discussion, as their effects on photon transmission in the system are negligible (refer to [Appendix C](#) for details). In this case, the squeezing pump field can be approximated as having no impact on the scattering of the incident photon, and the Hamiltonian is given by:

$$\begin{aligned} \mathcal{H}_2 = & \Delta_a a_{cw}^\dagger a_{cw} + i\sqrt{\kappa_{ex1}}(\varepsilon a_{cw}^\dagger - \varepsilon^* a_{cw}) + \Delta_m c^\dagger c \\ & + \Delta_b b_{ccw}^\dagger b_{ccw} + g_0(a_{cw}^\dagger b_{ccw} + a_{cw} b_{ccw}^\dagger) \\ & - J_0(a_{cw}^\dagger a_{cw} - b_{ccw}^\dagger b_{ccw})(c^\dagger + c), \end{aligned} \quad (7)$$

where $\Delta_b = \Delta_s^b - \Delta_p$. Comparing the Hamiltonians \mathcal{H}_1^s and \mathcal{H}_2 , due to directional quantum squeezing, the effective detuning of resonator R_B and the couplings are significantly different. If Δ_s^b is set to a small value, the effect of quantum squeezing on the detuning decreases, and the primary difference lies in the couplings.

In this work, we focus on single-photon transmission and the statistical properties of correlated photons. In the squeezing picture, the evolution of the entire system without squeezed-vacuum driving, as shown in Fig.1(a), can be characterized by the following master equation:

$$\begin{aligned} \frac{d\rho_1}{dt} = & -i[\mathcal{H}_1^s, \rho_1] + \kappa_a L[a_{ccw}]\rho_1 + \kappa_b L[b_{s,cw}]\rho_1 \\ & + \gamma_m(n_{th} + 1)L[c]\rho_1 + \gamma_m n_{th} L[c^\dagger]\rho_1 \\ & + \mathcal{L}_n[b_{s,cw}]\rho_1, \end{aligned} \quad (8)$$

where $L[o]\rho = 2o\rho o^\dagger - o^\dagger o\rho - \rho o^\dagger o$ is the Lindblad superoperator for operator o , and ρ_1 is the system density matrix. The total decay rates of resonators R_A and

R_B are $\kappa_a = \kappa_{ex1} + \kappa_i$ and $\kappa_b = \kappa_{ex2} + \kappa_i$, respectively. Here, κ_i is the intrinsic decay rate of the optical resonators, and κ_{ex2} is the external decay rate of resonator R_B . In the following, we assume $\kappa_a = \kappa_b = \kappa$ and $\Delta_a = \Delta_b = \Delta$ for simplicity. The decay rate of the mechanical resonator C is γ_m , and the mean thermal phonon number $n_{th} = 1/[\exp(\omega_m/k_B T) - 1]$, where k_B is the Boltzmann constant and T is the temperature of the reservoir at thermal equilibrium. The last term, $\mathcal{L}_n[b_{s,cw}]\rho_1$, describes the effective thermalization noise of the mode $b_{s,cw}$, which can be canceled by applying a broadband squeezed-vacuum field [38, 40, 50, 51] to reach the single-quantum level. Similarly, in Fig.1(b), the master equation is described as:

$$\begin{aligned}
 \frac{d\rho_2}{dt} = & -i[\mathcal{H}_2, \rho_2] + \kappa_a L[a_{cw}]\rho_2 + \kappa_b L[b_{ccw}]\rho_2 \\
 & + \gamma_m(n_{th} + 1)L[c]\rho_2 + \gamma_m n_{th} L[c^\dagger]\rho_2,
 \end{aligned} \tag{9}$$

where ρ_2 represents the density matrix of the system. It is worth noting that both types of photon detection channels are influenced by the environmental temperature T due to the presence of the mechanical oscillator. In this work, we neglect the presence of thermal photons in the optical system, as their number is typically negligible compared to that of phonons. Therefore, the thermal bath is unlikely to have a significant impact on the results.

According to the input-output relation, we have $a_{out} = \varepsilon - \sqrt{\kappa_{ex1}}a$ and $b_{out} = \sqrt{\kappa_{ex2}}b$. The single photon transmissions are defined as

$$T_{12/21} = \frac{\langle a_{out}^\dagger a_{out} \rangle}{\langle \varepsilon \varepsilon^* \rangle}, \quad T_{23} = \frac{\langle b_{out}^\dagger b_{out} \rangle}{\langle \varepsilon \varepsilon^* \rangle}, \tag{10}$$

where $\langle a_{out}^\dagger a_{out} \rangle$ and $\langle b_{out}^\dagger b_{out} \rangle$ are the mean photon numbers. $T_{12/21}$ represents the transmission from port 1 to port 2 or from port 2 to port 1, respectively, while T_{23} is the transmission from port 2 to port 3. The corresponding photon isolation ratio in the lower bus waveguide is defined as $\eta = 10 \log_{10}(T_{21}/T_{12})$.

3. Temperature sensitive nonreciprocal single photon transmission

There are two different mechanisms for the coupling between two optical resonators [51]. When $g_0 < \kappa$, the two resonators originally have no normal mode splitting (NMS). While for $g_0 > \kappa$, the system switches to the NMS scenario. To accurately illustrate how the squeezed coupling strength g_s influences the nonreciprocity of the system, assume the detuning Δ_s^b to be a small value. In Fig.3, we plot the single-photon transmission versus the detuning Δ for the no NMS scenario ($g_0 = 0.04\Delta_m$) and the NMS scenario ($g_0 = 0.4\Delta_m$), respectively. Since the value $\Delta_s^{a/b} = 0.01\Delta_m$ is small enough, the mode resonance shift induced by quantum squeezing can be neglected. In Fig.3(a), there is only one dip or peak in the single-photon transmission simulation curves, and no obvious nonreciprocity phenomenon is shown in the entire detuning range. On the contrary, for the NMS scenario in Fig.3(b), there are three main dips in both T_{12} and

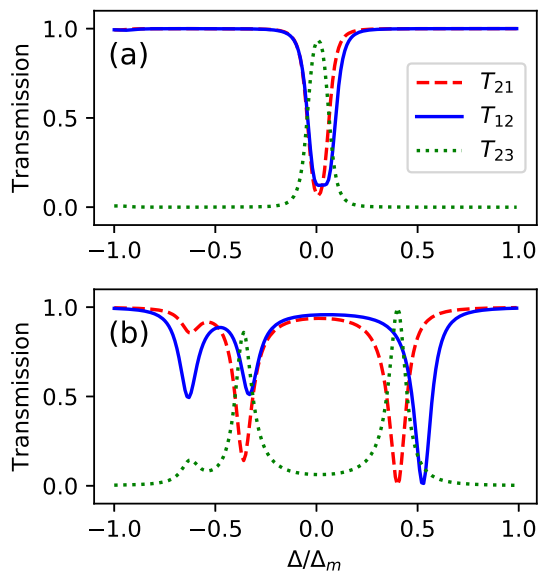


Figure 3. The transmittances T_{12} (blue solid line), T_{21} (red dashed line), and the transfer rate T_{23} (green dotted line) as functions of Δ are shown. (a) corresponds to the scenario without NMS ($g_0 = 0.04\Delta_m$); (b) represents the scenario with NMS ($g_0 = 0.4\Delta_m$). Other parameters are: $\kappa = 0.1\Delta_m$, $\gamma = 0.007\Delta_m$, $\varepsilon = 0.03\Delta_m$, $\Delta_s^{a/b} = 0.01\Delta_m$, $J_0 = 0.09\Delta_m$, $\beta = 0.9$, and $n_{\text{th}} = 0$.

T_{21} , indicating the system exhibits obvious single-photon nonreciprocal transmission characteristics, especially at the detuning $\Delta = g_\nu$ ($\nu = 0, s$). Additionally, it is always approximately true that $T_{21} + T_{23} = 1$. At the detuning $\Delta = g_0$, the single photon follows the transmission path $1 \rightarrow 2 \rightarrow 3$, indicating that the device operates as a three-port quasicirculator.

In this section, we explain the existence of dips in Fig.3(b). In the Hilbert space, $|n_a, n_b, n_c\rangle$ represents the Fock state with n_a (n_b) photons in resonator R_A (R_B) and n_c phonons in resonator C . Supposing the initial state $|\Delta\rangle$ is in a subspace formed by $\{|1, 0, 0\rangle, |1, 0, 1\rangle, |1, 0, 2\rangle, |0, 1, 0\rangle, |0, 1, 1\rangle, |0, 1, 2\rangle\}$, where we truncate the subspace to a maximum phonon number of two. Then the matrix form of the Hamiltonian \mathcal{H}_2 without the probe field part reads:

$$\begin{pmatrix} \Delta & -J_0 & 0 & g_0 & 0 & 0 \\ -J_0 & \Delta + \Delta_m & -\sqrt{2}J_0 & 0 & g_0 & 0 \\ 0 & -\sqrt{2}J_0 & \Delta + 2\Delta_m & 0 & 0 & g_0 \\ g_0 & 0 & 0 & \Delta & J_0 & 0 \\ 0 & g_0 & 0 & J_0 & \Delta + \Delta_m & \sqrt{2}J_0 \\ 0 & 0 & g_0 & 0 & \sqrt{2}J_0 & \Delta + 2\Delta_m \end{pmatrix} \quad (11)$$

Solving the above Hamiltonian, we obtain partial solutions corresponding to three dips of T_{21} in Fig.3(b), which are $\Delta_1 = 0.405\Delta_m$, $\Delta_2 = -0.364\Delta_m$, and $\Delta_3 = -0.627\Delta_m$. The eigenstate at Δ_1 is expressed as:

$$\begin{aligned}
 |\Delta_1\rangle \simeq \frac{1}{\mathcal{N}_1} & [\alpha_0(|1, 0, 0\rangle - |0, 1, 0\rangle) + \alpha_1(|1, 0, 1\rangle \\
 & + |0, 1, 1\rangle) + \alpha_2(|1, 0, 2\rangle - |0, 1, 2\rangle)], \tag{12}
 \end{aligned}$$

where $\alpha_0 = 314\alpha_2$ and $\alpha_1 = 16\alpha_2$, with \mathcal{N}_1 representing the normalization constant.

Similarly, the matrix form of the Hamiltonian \mathcal{H}_1^s without the probe field part reads:

$$\begin{pmatrix}
 \Delta & -J_0 & 0 & g_s & 0 & 0 \\
 -J_0 & \Delta + \Delta_m & -\sqrt{2}J_0 & 0 & g_s & 0 \\
 0 & -\sqrt{2}J_0 & \Delta + 2\Delta_m & 0 & 0 & g_s \\
 g_s & 0 & 0 & \Delta & J_s & 0 \\
 0 & g_s & 0 & J_s & \Delta + \Delta_m & \sqrt{2}J_s \\
 0 & 0 & g_s & 0 & \sqrt{2}J_s & \Delta + 2\Delta_m
 \end{pmatrix} \tag{13}$$

We also obtain partial solutions corresponding to three dips of T_{12} in Fig.3(b), which are $\Delta_1^s = 0.528\Delta_m$, $\Delta_2^s = -0.337\Delta_m$, and $\Delta_3^s = -0.635\Delta_m$. The eigenstate at Δ_1^s is expressed as:

$$\begin{aligned}
 |\Delta_1^s\rangle \simeq \frac{1}{\mathcal{N}_1^s} & (\alpha_{01}^s|1, 0, 0\rangle - \alpha_{02}^s|0, 1, 0\rangle + \alpha_{11}^s|1, 0, 1\rangle \\
 & + \alpha_{12}^s|0, 1, 1\rangle + \alpha_{21}^s|1, 0, 2\rangle - \alpha_{22}^s|0, 1, 2\rangle), \tag{14}
 \end{aligned}$$

where $\alpha_{01}^s = 247\alpha_{21}$, $\alpha_{02}^s = 253\alpha_{21}$, $\alpha_{11}^s = 3\alpha_{21}$, $\alpha_{12}^s = 34\alpha_{21}$, $\alpha_{22}^s = 4\alpha_{21}$, with \mathcal{N}_1^s representing the normalization constant. It is not difficult to see that the proportion of base vectors containing phonons is small for both cases.

The system is thermalized by mechanical noise. In Fig.4(a) and Fig.4(b), we plot the single-photon transmission versus the detuning Δ for $n_{\text{th}} = 0$ and $n_{\text{th}} = 10$, respectively. In the first case, at detunings Δ_1 and Δ_1^s , the corresponding isolation ratios are $\eta = -23$ dB and $\eta = 22.2$ dB, indicating strong nonreciprocity due to directional quantum squeezing in the low- n_{th} regime. However, as mechanical noise increases, the system's nonreciprocity is visibly impaired, with isolation ratios decreasing to $\eta = -3.3$ dB and $\eta = 1.1$ dB. These changes suggest that temperature significantly impacts the isolation effect of single photons. To better illustrate the system's photon transport response to temperature variations, we plot the transmission T_{21} at Δ_1 and T_{12} at Δ_1^s versus n_{th} in Fig.4(c). As n_{th} increases, single-photon transmission initially rises and eventually stabilizes around $n_{\text{th}} = 10$. This can be interpreted as follows: as the thermal phonon number increases, photon decoherence and scattering effects intensify, initially boosting the transmission probability. However, beyond a certain threshold, both the decoherence and scattering rates approach their saturation points. In other words, additional thermal noise no longer significantly increases coherence loss, and the photon scattering probability reaches a limit. As a result, the system's photonic transmission stabilizes, with the transmission probability becoming constant rather than continuing to vary with the thermal phonon number. Furthermore, directional

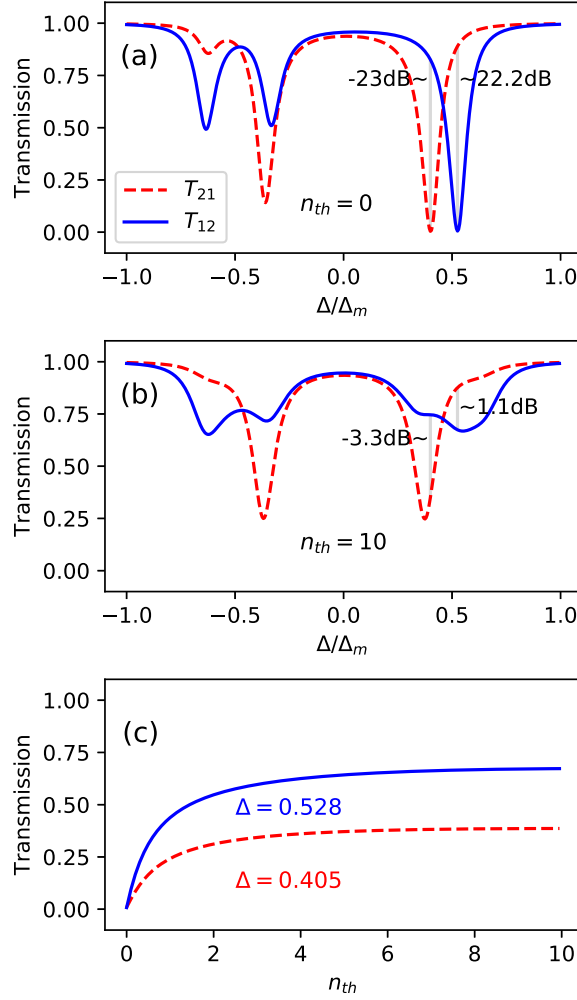


Figure 4. The transmittances T_{12} (blue solid line) and T_{21} (red dashed line) as functions of Δ for (a) $n_{th} = 0$ and (b) $n_{th} = 10$, respectively. In (c), the transmittances T_{12} at detuning $\Delta = 0.528\Delta_m$ and the transmittances T_{21} at detuning $\Delta = 0.405\Delta_m$ are plotted as functions of n_{th} . Other parameters are $\kappa = 0.1\Delta_m$, $\gamma = 0.007\Delta_m$, $\varepsilon = 0.03\Delta_m$, $\Delta_s^{a/b} = 0.01\Delta_m$, $g_0 = 0.4\Delta_m$, $J_0 = 0.09\Delta_m$, and $\beta = 0.9$.

parametric amplification enhances the optomechanical coupling strength J_s , making the transmission T_{12} particularly sensitive to changes in n_{th} .

In addition, the system's sensitivity to temperature varies depending on the location of resonator C. We plot the single-photon transmission versus the detuning Δ for $n_{th} = 0$ in Fig.5(a)(c) and for $n_{th} = 10$ in Fig.5(b)(d). The blue solid line represents resonator C placed in area I, the red dotted line represents it in area II, and the green dashed line represents it in area III. Comparing Fig.5(a) and Fig.5(b), we observe that resonator C in area I shows the strongest response. This is because photons in both the a -mode and b -mode are converted into phonons; a higher phonon conversion rate increases the system's sensitivity to temperature. In contrast, resonator C in area II shows a more pronounced response than in area III, as the directional parametric amplification

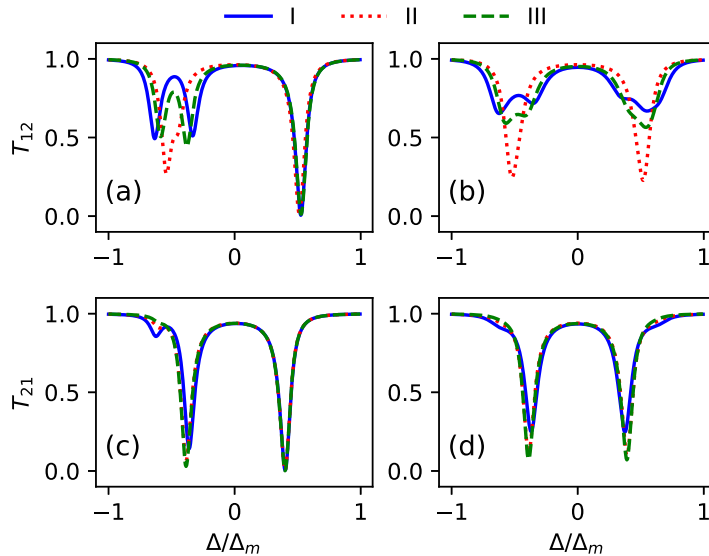


Figure 5. The transmittances T_{12} in (a) and (b), and T_{21} in (c) and (d) as functions of Δ for the case of the mechanical nanostring oscillator C being placed at area I (blue solid line), area II (red dotted line), and area III (green dashed line). In (a) and (c), $n_{\text{th}} = 0$; in (b) and (d), $n_{\text{th}} = 10$. Other parameters are $\kappa = 0.1\Delta_m$, $\gamma = 0.007\Delta_m$, $\varepsilon = 0.03\Delta_m$, $\Delta_s^{a/b} = 0.01\Delta_m$, $g_0 = 0.4\Delta_m$, $J_0 = 0.09\Delta_m$, and $\beta = 0.9$.

enhances the interaction between b -mode photons and phonons. Fig.5(c)(d) illustrates the case when the photon incidence direction is reversed. Here, the pump field does not interfere with photon transmission, and the position of resonator C has minimal impact on T_{21} , even with temperature changes.

4. Temperature sensitive nonreciprocal photon correlations

In this work, we use a coherent probe beam to drive the $\chi^{(2)}$ nonlinear microring systems [62], allowing us to study the response of the system's photon statistical properties to temperature. By applying the input-output relations, the statistical properties of the transmitted photons can be described by the second-order correlation functions as follows:

$$g_{12/21}^{(2)}(0) = \frac{\langle a_{\text{out}}^{\dagger 2} a_{\text{out}}^2 \rangle}{\langle a_{\text{out}}^{\dagger} a_{\text{out}} \rangle^2}, \quad (15)$$

where $g_{12/21}^{(2)}(0)$ is the equal-time second-order correlation function for the output photons from port 1 or port 2.

Based on the calculations in Section 3, we find that the eigenvectors with zero phonon number constitute a significant portion of the eigenstates, including $|\Delta_1\rangle$ and $|\Delta_1^s\rangle$. To approximate the two-photon resonance, we select the subspace $\{|2, 0\rangle, |1, 1\rangle, |0, 2\rangle\}$. The matrix forms of the Hamiltonians \mathcal{H}_2 and \mathcal{H}_1^s without the

probe field component are then given by

$$\begin{pmatrix} 2\Delta & \sqrt{2}g_\nu & 0 \\ \sqrt{2}g_\nu & 2\Delta & \sqrt{2}g_\nu \\ 0 & \sqrt{2}g_\nu & 2\Delta \end{pmatrix} \quad (16)$$

we obtain the solutions $\Delta_{\pm\nu} = \pm g_\nu$ and $\Delta' = 0$. The corresponding eigenstates are expressed as

$$|\Delta_{\pm\nu}\rangle = \frac{1}{\mathcal{N}_2}(|2, 0\rangle \pm \sqrt{2}|1, 1\rangle + |0, 2\rangle), \quad (17)$$

$$|\Delta'\rangle = \frac{1}{\mathcal{N}_3}(|2, 0\rangle + |0, 2\rangle), \quad (18)$$

where \mathcal{N}_2 and \mathcal{N}_3 are normalization constants. It's evident that Δ_ν represents both single and two-photon resonances of the system, making it an optimal point for detecting the statistical properties of photons in this quantum circulator. Conversely, in the case of $\Delta_{-\nu}$ and Δ' , the detection port exhibits both single-photon and two photon characteristics, resembling a coherent state.

In Fig.6, we depict the second-order correlation functions against the detuning Δ for $n_{\text{th}} = 0$ in Fig.6(a) and $n_{\text{th}} = 10$ in Fig.6(b), respectively. In the former case, numerical simulations reveal that $g_{21}^{(2)}(0) \gg 1$ and $g_{12}^{(2)}(0) \approx 1$ at $\Delta = \Delta_0$, while $g_{12}^{(2)}(0) \gg 1$ and $g_{21}^{(2)}(0) \approx 1$ at $\Delta = \Delta_s$. The transmitted photons exhibit a nonreciprocal strong bunching effect with low transmissibility since the single photons are transmitted to the upper drop waveguide ports. However, when $n_{\text{th}} = 10$, the statistical properties of the photons undergo significant changes, manifesting as a weak bunching effect. The physical explanation is that thermal phonons introduce phase and amplitude noise, enhance multi-phonon scattering, and induce decoherence, thereby disrupting the nonclassical statistical properties of the optical field. Consequently, the photon bunching effect is diminished, and the photon statistics tend to approach a Poisson distribution. In Fig.6(c), we illustrate the second-order correlation functions $g_{12}^{(2)}(0)$ at detuning $\Delta = 0.528\Delta_m$ and $g_{21}^{(2)}(0)$ at detuning $\Delta = 0.405\Delta_m$ against the mean thermal phonon number n_{th} . We observe that the correlation functions decrease exponentially before $n_{\text{th}} = 1$ and then remain constant near $n_{\text{th}} = 10$. Remarkably, the statistical properties of photons transmitted in the opposite directions exhibit no significant differences with changes in temperature, indicating that the directional quantum squeezing effect on improving photon statistics due to temperature is not apparent. This phenomenon contrasts with single-photon transmission. Furthermore, we examine the correlation functions corresponding to the location of resonator C in Fig.7. Comparing Fig.7(a) and Fig.7(b) at detuning $\Delta = 0.528\Delta_m$, and Fig.7(c) and Fig.7(d) at detuning $\Delta = 0.405\Delta_m$, we observe that the different locations of resonator C do not distinctly distinguish the statistical properties of photons, both exhibiting a transition from strong bunching effect at $n_{\text{th}} = 0$ to weak bunching effect at $n_{\text{th}} = 10$.

We further investigate the influence of the resonator-oscillator coupling strength J_0 on the nonreciprocity of the temperature-dependent system. In Fig.8, we illustrate

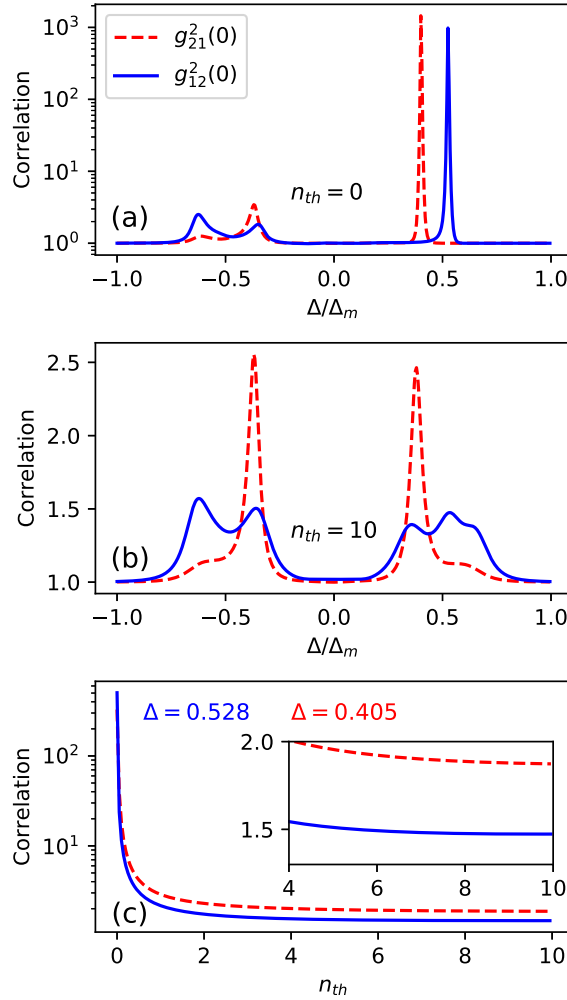


Figure 6. The equal time second-order correlation functions $g_{12}^2(0)$ (blue solid line) and $g_{21}^2(0)$ (red dashed line) as functions of Δ for (a) $n_{th} = 0$ and (b) $n_{th} = 10$, respectively. In (c), $g_{12}^2(0)$ at detuning $\Delta = 0.528\Delta_m$ and $g_{21}^2(0)$ at detuning $\Delta = 0.405\Delta_m$ are plotted as functions of n_{th} . Other parameters are $\kappa = 0.1\Delta_m$, $\gamma = 0.007\Delta_m$, $\varepsilon = 0.03\Delta_m$, $\Delta_s^{a/b} = 0.01\Delta_m$, $g_0 = 0.4\Delta_m$, $J_0 = 0.09\Delta_m$, and $\beta = 0.9$.

the single-photon transmission and correlation functions against J_0 for the cases of $n_{th} = 0$ and $n_{th} = 10$, respectively. In Fig.8(a) and Fig.8(c), for $n_{th} = 10$, the value of $T_{12/21}$ continuously increases until it approaches $J_0 = 1\Delta_m$. Conversely, for $n_{th} = 0$, the value of $T_{12/21}$ initially decreases before continuously increasing until it approaches $J_0 = 1\Delta_m$. This phenomenon can be explained by the fact that as J_0 increases, the exchange of photons and thermal phonons also increases, dissipating onto the mechanical oscillator. However, as J_0 further increases, oscillator C acts as a scattering center, re-scattering the b -mode photons originally emitted from port 4 or port 3 back into the resonant R_A , ultimately outputting to port 2 or port 1. The evolutionary behavior of $g_{12/21}^{(2)}(0)$ in Fig.8(b) and Fig.8(d) corresponds to the single-photon transmission case discussed earlier. Additionally, analyzing Fig.8(a) and Fig.8(b), we find that the

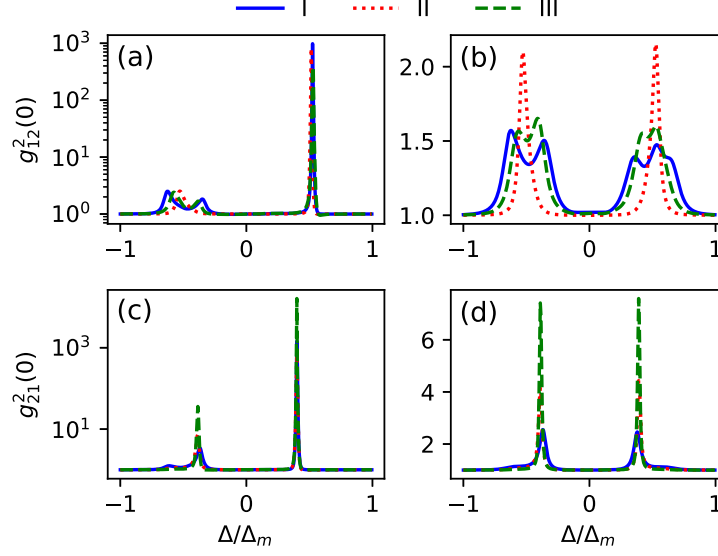


Figure 7. The equal-time second-order correlation functions $g_{12}^2(0)$ in (a) and (b) and $g_{21}^2(0)$ in (c) and (d) as functions of Δ for the mechanical nanostring oscillator C placed in area I (blue solid line), area II (red dotted line), and area III (green dashed line). In (a) and (c), $n_{th} = 0$; in (b) and (d), $n_{th} = 10$. Other parameters are $\kappa = 0.1\Delta_m$, $\gamma = 0.007\Delta_m$, $\varepsilon = 0.03\Delta_m$, $\Delta_s^{a/b} = 0.01\Delta_m$, $g_0 = 0.4\Delta_m$, $J_0 = 0.09\Delta_m$, and $\beta = 0.9$.

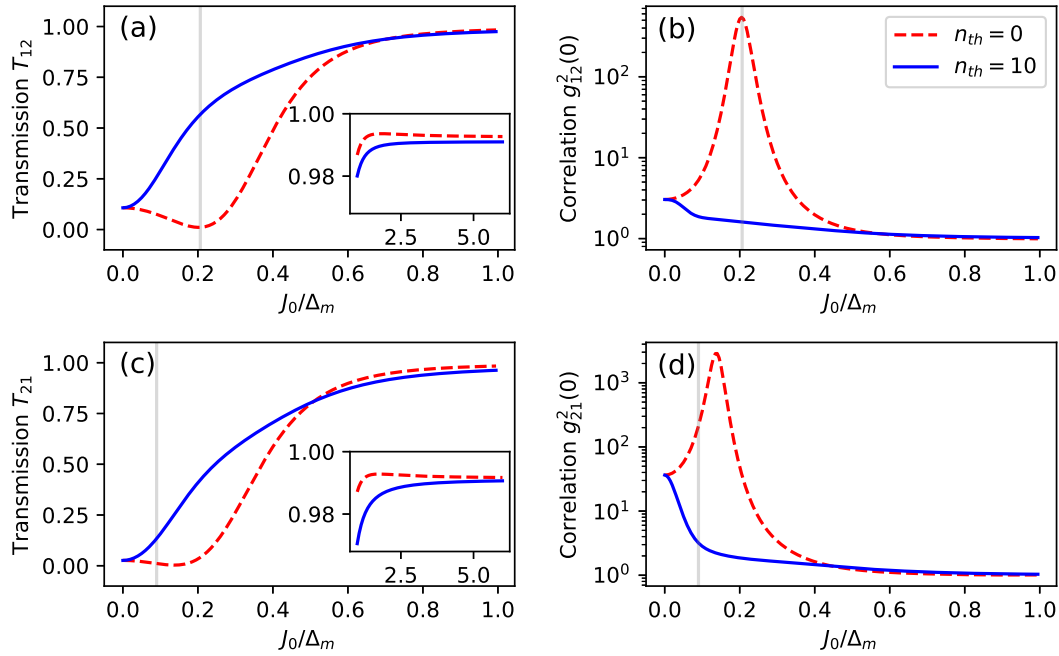


Figure 8. The transmittances T_{12} in (a) and T_{21} in (b) as functions of the resonator-oscillator coupling strength J_0 , with the oscillator C placed in area III. The equal-time second-order correlation function $g_{12}^2(0)$ in (c) and $g_{21}^2(0)$ in (d) as functions of J_0 . The red dashed line represents $n_{th} = 0$ and the blue solid line represents $n_{th} = 10$. The detuning in (a) and (b) is $\Delta = 0.528\Delta_m$, while in (c) and (d) it is $\Delta = 0.405\Delta_m$. Other parameters are $\kappa = 0.1\Delta_m$, $\gamma = 0.007\Delta_m$, $\varepsilon = 0.03\Delta_m$, $g_0 = 0.4\Delta_m$, and $\beta = 0.9$.

suitable coupling strength arises at around $J_0 = 0.09\Delta_m$, where T_{12} and $g_{12}^{(2)}(0)$ are most responsive to temperature simultaneously. The corresponding effective coupling strength is $J_s = 0.206\Delta_m$. However, for T_{21} and $g_{21}^{(2)}(0)$ in Fig.8(c) and Fig.8(d), the most responsive point to temperature is not achieved, since the coupling strength for this case is not enhanced.

5. Experimental feasibility

The thin-film material lithium niobate [63–65] has been extensively utilized to fabricate $\chi^{(2)}$ nonlinearity resonators. Recent advancements have led to the development of high-Q whispering gallery resonators on-chip, reaching Q-factors as high as 3×10^6 . Additionally, epitaxial aluminum nitride has emerged as a promising photonic platform, showcasing efficient $\chi^{(2)}$ and $\chi^{(3)}$ nonlinear processes [66, 67]. It stands as a strong alternative to traditional lithium niobate materials. Silicon has enabled the creation of ring resonators with unprecedentedly small sizes. Microring resonators and waveguides made of silicon are typically fabricated using techniques like e-beam or optical lithography and reactive ion etching, often employing CMOS manufacturing tools [68, 69]. In our proposed scheme, the prevalent method of coupling light from a waveguide to a ring resonator or between ring resonators is through a directional coupler [70].

The whispering-gallery-mode optomechanical system enables the evanescent coupling of nanomechanical oscillators to an optical microresonator. This has been demonstrated in various setups, such as a tapered-fibre-interfaced optical microresonator dispersively coupled to an array of nanomechanical oscillators. For instance, doubly clamped SiN nanostring oscillators with dimensions of $110 \text{ nm} \times (300\text{-}500) \text{ nm} \times (15\text{-}40) \mu\text{m}$ have been utilized for this purpose [11]. Additionally, a high-stress Si_3N_4 nanomechanical beam integrated into the evanescent mode volume of a SiO_2 microdisk has been employed [12]. Apart from the traditional minimal model (i.e., one optical mode coupled to one mechanical mode) of cavity optomechanics, it is theoretically feasible to extend to multimode optomechanics, as discussed in Ref. [4].

Broadband squeezed-vacuum fields have proven to be an effective strategy for mitigating quantum noise, and they are currently utilized in advanced detectors. In recent experiments, a suspended 300-meter-long filter cavity capable of inducing a rotation of the squeezing ellipse below 100 Hz has demonstrated the reduction of quantum noise in advanced gravitational-wave detectors across their entire observation bandwidth [71]. Another study achieved broadband reduction of quantum radiation pressure noise [72]. In addition to these applications, broadband squeezed-vacuum fields have been employed in various physics experiments, including the suppression of radiative decay of atoms [73], squeezing of mechanical modes in optomechanical systems [74], and the creation of squeezed lasing [75], among others.

6. Conclusion

We have successfully demonstrated nonreciprocal single-photon transmission and quantum correlations in temperature-sensitive optomechanical systems, where the nonreciprocity arises from directional quantum squeezing. Our findings reveal that the nonreciprocity of the system is significantly influenced by thermal phonons. Specifically, at detuning $\Delta = 0.528\Delta_m$ (or $\Delta = 0.405\Delta_m$), when $n_{\text{th}} = 0$, the configuration behaves like a diode with a high isolation ratio, and the statistical properties of the transmitted photons exhibit a strong bunching effect. Conversely, for $n_{\text{th}} = 10$, the isolation of the system is greatly reduced from 22.2 dB to 1.1 dB (or from -23 dB to -3.3 dB), and the statistical properties of the transmitted photons exhibit a weak bunching effect. Moreover, our setup benefits from directional parametric amplification, which enhances the optomechanical coupling strength. This enhancement makes the system more sensitive to temperature, making it suitable for precise temperature measurements at ultralow temperatures. For instance, we can use the values of the single-photon transmission rate or the equal-time second-order correlation function at detuning Δ_1 and detuning Δ_1^s as temperature indicators. In conclusion, our research provides a scheme for achieving optical nonreciprocity in chip-compatible magnetic-free devices, enabling backaction-immune quantum measurement and chiral quantum photonics. Furthermore, our work has the potential to be extended to phonon systems, allowing for applications such as phonon blockades [76, 77] and nonreciprocal phonon lasers [78, 79].

Acknowledgments

This work is supported by the National Natural Science Foundation of China under Grant No. 12375018.

Data availability statement

The data that support the findings of this study are available upon reasonable request from the authors.

Appendix A: Optomechanically coupled to two optical resonators with coupling strengths of opposite signs

The equivalent schematic diagram of Fig. 1 is shown in Fig. A. It is worth noting that the walls of the microring resonators in Fig. 1 are fixed (which contrasts with the configuration in Ref. [60], where the system can be stretched or compressed), meaning the frequencies of the optical modes ω_a and ω_b remain unchanged. However, we have demonstrated that the configuration in Fig. 1 is mathematically equivalent to the configuration in Fig. A.

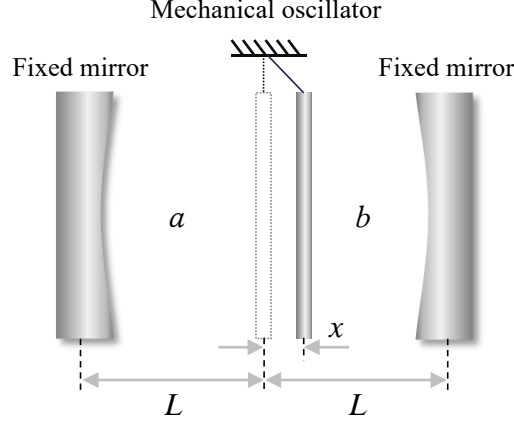


Figure A. Equivalent schematic diagram of Fig. 1. The optical cavity is divided into cavity a and cavity b by the central mechanical oscillator. At rest, the distance between the mechanical oscillator and the fixed mirrors at both ends is L .

The resonant frequency of the cavity field is closely related to the cavity length. When the mechanical oscillator vibrates near its equilibrium position, the corresponding cavity length becomes $L \rightarrow L \pm x$, causing a shift in the cavity mode frequency [80].

$$\begin{aligned}\omega_a(L+x) &= \frac{\pi c}{L+x}, \\ \omega_b(L-x) &= \frac{\pi c}{L-x},\end{aligned}\tag{A1}$$

where c denotes the speed of light in a vacuum.

In general, the displacement of the macroscopic oscillator is much smaller than the length of the optical cavity at rest, i.e., $x \ll L$, as described by the Taylor expansion formula

$$\begin{aligned}\omega_a(L+x) &= \frac{\pi c}{L} \times \frac{1}{1+x/L} = \frac{\pi c}{L} \left(1 - \frac{x}{L} + \frac{x^2}{L^2} - \dots\right) \\ &\approx \omega_a(L) \left(1 - \frac{x}{L}\right), \\ \omega_b(L-x) &= \frac{\pi c}{L} \times \frac{1}{1-x/L} = \frac{\pi c}{L} \left(1 + \frac{x}{L} + \frac{x^2}{L^2} + \dots\right) \\ &\approx \omega_b(L) \left(1 + \frac{x}{L}\right).\end{aligned}\tag{A2}$$

When the optical field is driven by an external laser, the photons couple with the oscillator, and the total Hamiltonian of the system is given by

$$\begin{aligned}H_A + H_B + H_{int} &= \omega_a(L+x)a^\dagger a + \omega_b(L-x)b^\dagger b \\ &= \omega_a(L)a^\dagger a + \omega_b(L)b^\dagger b \\ &\quad - \omega_a(L)\frac{x}{L}a^\dagger a + \omega_b(L)\frac{x}{L}b^\dagger b.\end{aligned}\tag{A3}$$

The equation indicates that the free Hamiltonian of the optical modes H_A and H_B can be considered constant, corresponding to the scenario shown in Fig. 1. Substituting $x = \sqrt{\frac{1}{2m\omega_m}}(c + c^\dagger)$ (where m is the effective mass of the mechanical oscillator) into the equation and assuming $\omega_a(L) = \omega_b(L) = \omega(L)$, we obtain:

$$H_{int} = -\frac{\omega(L)}{L}(a^\dagger a - b^\dagger b)x = -J'_0(a^\dagger a - b^\dagger b)(c + c^\dagger), \quad (\text{A4})$$

where $J'_0 = \sqrt{\frac{1}{2m\omega_m}} \frac{\omega(L)}{L}$.

Appendix B: Detailed solution of Eq. 6

When transforming the system into the squeezing picture, we should only substitute b_{cw} (b_{cw}^\dagger) in Eq.5. Thus, the Hamiltonian we need to consider simplifies to

$$\begin{aligned} \mathcal{H} = & \Delta_s^b b_{cw}^\dagger b_{cw} + \frac{\Omega}{2}(b_{cw}^{\dagger 2} + b_{cw}^2) + g_0(a_{ccw}^\dagger b_{cw} + a_{ccw} b_{cw}^\dagger) \\ & + J_0 b_{cw}^\dagger b_{cw} (c^\dagger + c). \end{aligned} \quad (\text{B1})$$

By applying the Bogoliubov squeezing transformation $b_{cw} = \cosh(r_s)b_{s,cw} - \sinh(r_s)b_{s,cw}^\dagger$ and the commutation relation $[b_{s,cw}, b_{s,cw}^\dagger] = 1$ to Eq. B1, neglecting the parametric interaction term $J_0 \sinh(2r_s)(b_{s,cw}^{\dagger 2} + b_{s,cw}^2)(c^\dagger + c)/2$, and under the rotating-wave approximation while neglecting the counter-rotating terms, the Hamiltonian becomes

$$\begin{aligned} \mathcal{H}^s = & [\Delta_s^b \cosh(2r_s) - \Omega \sinh(2r_s)] b_{s,cw}^\dagger b_{s,cw} \\ & + \left[\frac{\Omega}{2} \cosh(2r_s) - \frac{\Delta_s^b}{2} \sinh(2r_s) \right] (b_{s,cw}^{\dagger 2} + b_{s,cw}^2) \\ & + [J_s b_{s,cw}^\dagger b_{s,cw} + J_0 \sinh^2(r_s)] (c^\dagger + c) \\ & + g_s (a_{ccw}^\dagger b_{s,cw} + a_{ccw} b_{s,cw}^\dagger) \\ & + \Delta_s^b \sinh^2(r_s) - \frac{\Omega}{2} \sinh(2r_s), \end{aligned} \quad (\text{B2})$$

neglecting the last constant term, and in the frame rotating at the frequency Δ_p , the above equation becomes

$$\begin{aligned} \mathcal{H}^s = & \Delta_s^s b_{s,cw}^\dagger b_{s,cw} + g_s (a_{ccw}^\dagger b_{s,cw} + a_{ccw} b_{s,cw}^\dagger) \\ & + [J_s b_{s,cw}^\dagger b_{s,cw} + J_0 \sinh^2(r_s)] (c^\dagger + c). \end{aligned} \quad (\text{B3})$$

The last term, which applies to the mechanical oscillator, can be canceled by applying a constant force F . The remaining unchanged terms from Eq. 5 are then incorporated, leading to the final form presented in Eq. 6.

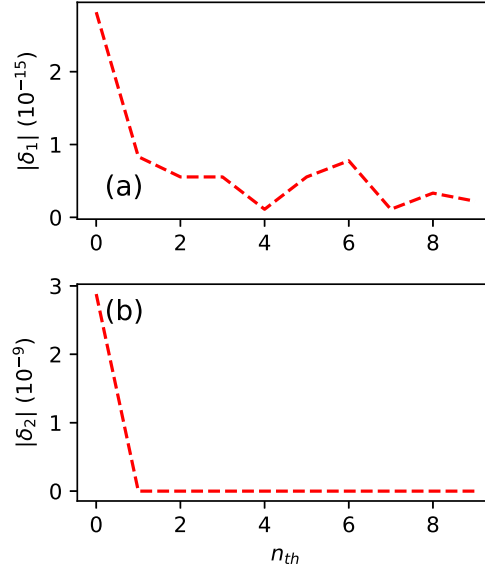


Figure C1. The parameters $|\delta_1|$ and $|\delta_2|$ as functions of n_{th} at a detuning of $\Delta = 0.528\Delta_m$. The other parameters are $\kappa = 0.1\Delta_m$, $\gamma = 0.007\Delta_m$, $\varepsilon = 0.03\Delta_m$, $\Delta_s^{a/b} = 0.01\Delta_m$, $g_0 = 0.4\Delta_m$, $J_0 = 0.09\Delta_m$, and $\beta = 0.9$.

Appendix C: The effect of the omitted optomechanical coupling terms on photon transmission

In this section, we incorporate the coupling of oscillator C with the CCW mode in R_B and the CW mode in R_A into the system when a photon is incident from port 1. The corresponding Hamiltonian in the squeezing picture is given by:

$$\begin{aligned}
 (\mathcal{H}_1^s)' &= \mathcal{H}_1^s + \Delta_a a_{cw}^\dagger a_{cw} + \Delta_b b_{ccw}^\dagger b_{ccw} + g_0 (a_{cw}^\dagger b_{ccw} + a_{cw} b_{ccw}^\dagger) \\
 &\quad - (J_0 a_{cw}^\dagger a_{cw} - J_0 b_{ccw}^\dagger b_{ccw})(c^\dagger + c).
 \end{aligned}
 \tag{C1}$$

Similar improvements need to be made to the master equation, where we must account for the dissipation of photons in these two modes as:

$$\begin{aligned}
 \frac{d\rho_1'}{dt} &= -i[(\mathcal{H}_1^s)', \rho_1'] + \kappa_a L[a_{ccw}] \rho_1' + \kappa_a L[a_{cw}] \rho_1' + \kappa_b L[b_{s,cw}] \rho_1' + \kappa_b L[b_{ccw}] \rho_1' \\
 &\quad + \gamma_m (n_{th} + 1) L[c] \rho_1' + \gamma_m n_{th} L[c^\dagger] \rho_1' \\
 &\quad + \mathcal{L}_n[b_{s,cw}] \rho_1'.
 \end{aligned}
 \tag{C2}$$

From the complete Hamiltonian and master equation above, we obtain the single-photon transmission T'_{12} and the second-order correlation function $g'_{12}(0)$. We then define $\delta_1 = T_{12} - T'_{12}$ and $\delta_2 = g_{12}(0) - g'_{12}(0)$ to evaluate the difference in photon transmission between the two systems. In Fig. C1, we plot the parameters $|\delta_1|$ and $|\delta_2|$ as functions of n_{th} at a detuning of $\Delta = 0.528\Delta_m$. It is evident that these two

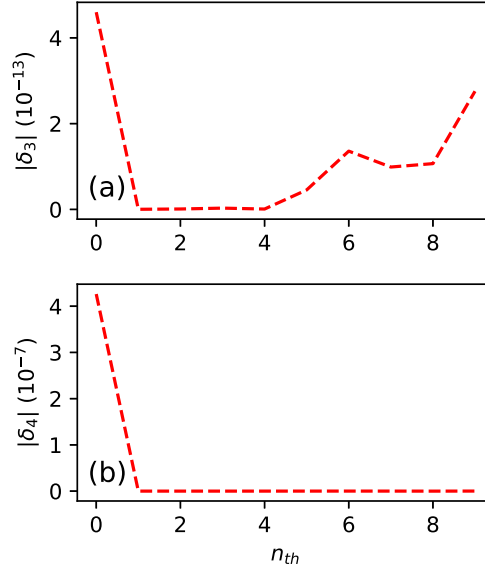


Figure C2. The parameters $|\delta_3|$ and $|\delta_4|$ as functions of n_{th} at a detuning of $\Delta = 0.405\Delta_m$. The other parameters are $\kappa = 0.1\Delta_m$, $\gamma = 0.007\Delta_m$, $\varepsilon = 0.03\Delta_m$, $\Delta_s^{a/b} = 0.01\Delta_m$, $g_0 = 0.4\Delta_m$, $J_0 = 0.09\Delta_m$, and $\beta = 0.9$.

parameters are of the order of 10^{-15} and 10^{-9} , respectively, indicating that there is little difference between the two systems in terms of single-photon transmission and photon statistical properties. Therefore, the two optomechanical coupling terms omitted in the main text have a minimal impact on our observed photon transmission effects and can be safely neglected.

Similarly, when a photon is incident from port 2, with an additional force F applied to oscillator C , the corresponding Hamiltonian in the squeezing picture is given by:

$$\begin{aligned}
 (\mathcal{H}_2^s)' &= \mathcal{H}_2 + \Delta_a a_{ccw}^\dagger a_{ccw} + \Delta_b^s b_{cw}^\dagger b_{cw} + g_s (a_{ccw}^\dagger b_{cw} + a_{ccw} b_{cw}^\dagger) \\
 &\quad - (J_0 a_{ccw}^\dagger a_{ccw} - J_s b_{cw}^\dagger b_{cw}) (c^\dagger + c).
 \end{aligned}
 \tag{C3}$$

For the master equation, it is sufficient to replace $(\mathcal{H}_1^s)'$ with $(\mathcal{H}_2^s)'$ and ρ_1' with ρ_2' in Eq. C2. Based on these, we obtain the single-photon transmission T_{21}' and the second-order correlation function $g'_{21}(0)$. We then define $\delta_3 = T_{21} - T_{21}'$ and $\delta_4 = g_{21}(0) - g'_{21}(0)$ to evaluate the difference in photon transmission between the two systems as before. In Fig. C2, we plot the parameters $|\delta_3|$ and $|\delta_4|$ as functions of n_{th} at a detuning of $\Delta = 0.405\Delta_m$. The simulation results indicate that these two parameters are on the order of 10^{-13} and 10^{-7} , respectively. Consequently, the corresponding optomechanical coupling terms can be safely neglected.

References

- [1] Kippenberg T J and Vahala K J 2008 *Science* **321** 1172–1176 URL <https://www.science.org/doi/abs/10.1126/science.1156032>

- [2] Ludwig M, Safavi-Naeini A H, Painter O and Marquardt F 2012 *Phys. Rev. Lett.* **109**(6) 063601 URL <https://link.aps.org/doi/10.1103/PhysRevLett.109.063601>
- [3] Wang Y D and Clerk A A 2013 *Phys. Rev. Lett.* **110**(25) 253601 URL <https://link.aps.org/doi/10.1103/PhysRevLett.110.253601>
- [4] Aspelmeyer M, Kippenberg T J and Marquardt F 2014 *Rev. Mod. Phys.* **86**(4) 1391–1452 URL <https://link.aps.org/doi/10.1103/RevModPhys.86.1391>
- [5] Xu H, Mason D, Jiang L and Harris J 2016 *Nature* **537** 80–83 URL <https://www.nature.com/articles/nature18604>
- [6] Li J, Zhou Z H, Wan S, Zhang Y L, Shen Z, Li M, Zou C L, Guo G C and Dong C H 2022 *Phys. Rev. Lett.* **129**(6) 063605 URL <https://link.aps.org/doi/10.1103/PhysRevLett.129.063605>
- [7] Wang B, Nori F and Xiang Z L 2024 *Phys. Rev. Lett.* **132**(5) 053601 URL <https://link.aps.org/doi/10.1103/PhysRevLett.132.053601>
- [8] Jansen M, Tisdale W A and Wood V 2023 *Nat. Mater.* **22** 161–169 URL <https://www.nature.com/articles/s41563-022-01438-4>
- [9] Woolf D, Hui P C, Iwase E, Khan M, Rodriguez A W, Deotare P, Bulu I, Johnson S G, Capasso F and Loncar M 2013 *Opt. Express* **21** 7258–7275 URL <https://opg.optica.org/oe/fulltext.cfm?uri=oe-21-6-7258&id=250903>
- [10] Dong C, Fiore V, Kuzyk M C and Wang H 2013 *Phys. Rev. A* **87**(5) 055802 URL <https://link.aps.org/doi/10.1103/PhysRevA.87.055802>
- [11] Anetsberger G, Arcizet O, Unterreithmeier Q P, Rivière R, Schliesser A, Weig E M, Kotthaus J P and Kippenberg T J 2009 *Nat. Phys.* **5** 909–914 URL <https://www.nature.com/articles/nphys1425>
- [12] Schilling R, Schütz H, Ghadimi A H, Sudhir V, Wilson D J and Kippenberg T J 2016 *Phys. Rev. Appl.* **5**(5) 054019 URL <https://link.aps.org/doi/10.1103/PhysRevApplied.5.054019>
- [13] Lodahl P, Mahmoodian S, Stobbe S, Rauschenbeutel A, Schneeweiss P, Volz J, Pichler H and Zoller P 2017 *Nature* **541** 473–480 URL <https://www.nature.com/articles/nature21037>
- [14] O’Shea D, Junge C, Volz J and Rauschenbeutel A 2013 *Phys. Rev. Lett.* **111**(19) 193601 URL <https://link.aps.org/doi/10.1103/PhysRevLett.111.193601>
- [15] Junge C, O’Shea D, Volz J and Rauschenbeutel A 2013 *Phys. Rev. Lett.* **110**(21) 213604 URL <https://link.aps.org/doi/10.1103/PhysRevLett.110.213604>
- [16] Xia K, Lu G, Lin G, Cheng Y, Niu Y, Gong S and Twamley J 2014 *Phys. Rev. A* **90**(4) 043802 URL <https://link.aps.org/doi/10.1103/PhysRevA.90.043802>
- [17] Tang L, Tang J, Zhang W, Lu G, Zhang H, Zhang Y, Xia K and Xiao M 2019 *Phys. Rev. A* **99**(4) 043833 URL <https://link.aps.org/doi/10.1103/PhysRevA.99.043833>
- [18] Zheng J C and Li P B 2023 *Opt. Express* **31** 21881–21898 URL <https://opg.optica.org/oe/fulltext.cfm?uri=oe-31-13-21881&id=531691>
- [19] Hafezi M and Rabl P 2012 *Opt. Express* **20** 7672–7684 URL <https://opg.optica.org/oe/fulltext.cfm?uri=oe-20-7-7672&id=230462>
- [20] Shen Z, Zhang Y L, Chen Y, Sun F W, Zou X B, Guo G C, Zou C L and Dong C H 2018 *Nat. Commun.* **9** 1–6 URL <https://www.nature.com/articles/s41467-018-04187-8>
- [21] Shen Z, Zhang Y L, Chen Y, Zou C L, Xiao Y F, Zou X B, Sun F W, Guo G C and Dong C H 2016 *Nat. Commun.* **10** 657–661 URL <https://www.nature.com/articles/nphoton.2016.161>
- [22] Ruesink F, Miri M A, Alu A and Verhagen E 2016 *Nat. Commun.* **7** 13662 URL <https://www.nature.com/articles/ncomms13662>
- [23] Ruesink F, Mathew J P, Miri M A, Alù A and Verhagen E 2018 *Nat. Commun.* **9** 1–6 URL <https://www.nature.com/articles/s41467-018-04202-y>
- [24] Xu X, Zhao Y, Wang H, Jing H and Chen A 2020 *Photon. Res.* **8** 143–150 URL <https://opg.optica.org/prj/fulltext.cfm?uri=prj-8-2-143&id=426096>
- [25] Caloz C, Alù A, Tretyakov S, Sounas D, Achouri K and Deck-Léger Z L 2018 *Phys. Rev. Appl.* **10**(4) 047001 URL <https://link.aps.org/doi/10.1103/PhysRevApplied.10.047001>
- [26] Nassar H, Yousefzadeh B, Fleury R, Ruzzene M, Alù A, Daraio C, Norris A N, Huang G and

- Haberman M R 2020 *Nat. Rev. Mater.* **5** 667–685 URL <https://www.nature.com/articles/s41578-020-0206-0>
- [27] Gou W, Chen T, Xie D, Xiao T, Deng T S, Gadway B, Yi W and Yan B 2020 *Phys. Rev. Lett.* **124**(7) 070402 URL <https://link.aps.org/doi/10.1103/PhysRevLett.124.070402>
- [28] Kutsaev S V, Krasnok A, Romanenko S N, Smirnov A Y, Taletski K and Yakovlev V P 2021 *Adv. Photonics Res.* **2** 2000104 URL <https://onlinelibrary.wiley.com/doi/full/10.1002/adpr.202000104>
- [29] Ren Y l, Ma S l, Xie J k, Li X k, Cao M t and Li F l 2022 *Phys. Rev. A* **105**(1) 013711 URL <https://link.aps.org/doi/10.1103/PhysRevA.105.013711>
- [30] Wang Y X, Wang C and Clerk A A 2023 *PRX Quantum* **4**(1) 010306 URL <https://link.aps.org/doi/10.1103/PRXQuantum.4.010306>
- [31] Zheng J C, Dong X L, Chen J Q, Hei X L, Pan X F, Yao X Y, Ren Y M, Qiao Y F and Li P B 2024 *Phys. Rev. A* **109**(6) 063709 URL <https://link.aps.org/doi/10.1103/PhysRevA.109.063709>
- [32] Esteve J, Gross C, Weller A, Giovanazzi S and Oberthaler M K 2008 *Nature* **455** 1216–1219 URL <https://www.nature.com/articles/nature07332>
- [33] Drummond P D and Ficek Z 2013 *Quantum squeezing* vol 27 (Springer Science & Business Media) URL <https://books.google.com/books?hl=zh-CN&lr=&id=VSzrCAAQBAJ&oi=fnd&pg=PR14&dq=quantum+squeezing&ots=LcbAgoPDsj&sig=eRdl0-r5Mc1UkkBI12k94pfXoEw#v=onepage&q=quantum%20squeezing&f=false>
- [34] Ma J, Wang X, Sun C P and Nori F 2011 *Phys. Rep.* **509** 89–165 URL <https://www.sciencedirect.com/science/article/abs/pii/S0370157311002201>
- [35] Braunstein S L 2005 *Phys. Rev. A* **71**(5) 055801 URL <https://link.aps.org/doi/10.1103/PhysRevA.71.055801>
- [36] Qin W, Miranowicz A, Jing H and Nori F 2021 *Phys. Rev. Lett.* **127**(9) 093602 URL <https://link.aps.org/doi/10.1103/PhysRevLett.127.093602>
- [37] Qin W, Miranowicz A and Nori F 2022 *Phys. Rev. Lett.* **129**(12) 123602 URL <https://link.aps.org/doi/10.1103/PhysRevLett.129.123602>
- [38] Qin W, Miranowicz A, Li P B, Lü X Y, You J Q and Nori F 2018 *Phys. Rev. Lett.* **120**(9) 093601 URL <https://link.aps.org/doi/10.1103/PhysRevLett.120.093601>
- [39] Chen Y H, Qin W, Wang X, Miranowicz A and Nori F 2021 *Phys. Rev. Lett.* **126**(2) 023602 URL <https://link.aps.org/doi/10.1103/PhysRevLett.126.023602>
- [40] Qin W, Macrì V, Miranowicz A, Savasta S and Nori F 2019 *Phys. Rev. A* **100**(6) 062501 URL <https://link.aps.org/doi/10.1103/PhysRevA.100.062501>
- [41] Barnett S and Knight P 1987 *J. Mod. Opt.* **34** 841–853 URL <https://www.tandfonline.com/doi/abs/10.1080/09500348714550781>
- [42] Wineland D J, Bollinger J J, Itano W M, Moore F L and Heinzen D J 1992 *Phys. Rev. A* **46**(11) R6797–R6800 URL <https://link.aps.org/doi/10.1103/PhysRevA.46.R6797>
- [43] Wollman E E, Lei C, Weinstein A, Suh J, Kronwald A, Marquardt F, Clerk A A and Schwab K 2015 *Science* **349** 952–955 URL <https://www.science.org/doi/abs/10.1126/science.aac5138>
- [44] Pirkkalainen J M, Damskäg E, Brandt M, Massel F and Sillanpää M A 2015 *Phys. Rev. Lett.* **115**(24) 243601 URL <https://link.aps.org/doi/10.1103/PhysRevLett.115.243601>
- [45] Lei C U, Weinstein A J, Suh J, Wollman E E, Kronwald A, Marquardt F, Clerk A A and Schwab K C 2016 *Phys. Rev. Lett.* **117**(10) 100801 URL <https://link.aps.org/doi/10.1103/PhysRevLett.117.100801>
- [46] Lawrie B J, Lett P D, Marino A M and Pooser R C 2019 *Acs Photonics* **6** 1307–1318 URL <https://pubs.acs.org/doi/abs/10.1021/acsp Photonics.9b00250>
- [47] Xu C, Zhang L, Huang S, Ma T, Liu F, Yonezawa H, Zhang Y and Xiao M 2019 *Photon. Res.* **7** A14–A26 URL <https://opg.optica.org/prj/fulltext.cfm?uri=prj-7-6-A14&id=412100>
- [48] Ganapathy D, Jia W, Nakano M, Xu V, Aritomi N and et al (LIGO O4 Detector Collaboration) 2023 *Phys. Rev. X* **13**(4) 041021 URL <https://link.aps.org/doi/10.1103/PhysRevX.13.041021>

041021

- [49] Lu B, Liu L, Song J Y, Wen K and Wang C 2023 *AAPPS Bull.* **33** 7 URL <https://link.springer.com/article/10.1007/s43673-023-00077-4>
- [50] Lü X Y, Wu Y, Johansson J R, Jing H, Zhang J and Nori F 2015 *Phys. Rev. Lett.* **114**(9) 093602 URL <https://link.aps.org/doi/10.1103/PhysRevLett.114.093602>
- [51] Tang L, Tang J, Chen M, Nori F, Xiao M and Xia K 2022 *Phys. Rev. Lett.* **128**(8) 083604 URL <https://link.aps.org/doi/10.1103/PhysRevLett.128.083604>
- [52] Shen C P, Chen J Q, Pan X F, Ren Y M, Dong X L, Hei X L, Qiao Y F and Li P B 2023 *Phys. Rev. A* **108**(2) 023716 URL <https://link.aps.org/doi/10.1103/PhysRevA.108.023716>
- [53] Zueco D, Reuther G M, Kohler S and Hänggi P 2009 *Phys. Rev. A* **80**(3) 033846 URL <https://link.aps.org/doi/10.1103/PhysRevA.80.033846>
- [54] Liu Y x, Miranowicz A, Gao Y B, Bajaj J c v, Sun C P and Nori F 2010 *Phys. Rev. A* **82**(3) 032101 URL <https://link.aps.org/doi/10.1103/PhysRevA.82.032101>
- [55] Liang B, Yuan B and Cheng J c 2009 *Phys. Rev. Lett.* **103**(10) 104301 URL <https://link.aps.org/doi/10.1103/PhysRevLett.103.104301>
- [56] Maznev A, Every A and Wright O 2013 *Wave Motion* **50** 776–784 URL <https://www.sciencedirect.com/science/article/abs/pii/S016521251300036X>
- [57] Li X F, Ni X, Feng L, Lu M H, He C and Chen Y F 2011 *Phys. Rev. Lett.* **106**(8) 084301 URL <https://link.aps.org/doi/10.1103/PhysRevLett.106.084301>
- [58] Darabi A, Fang L, Mojahed A, Fronk M D, Vakakis A F and Leamy M J 2019 *Phys. Rev. B* **99**(21) 214305 URL <https://link.aps.org/doi/10.1103/PhysRevB.99.214305>
- [59] Liu C, Du Z, Sun Z, Gao H and Guo X 2015 *Phys. Rev. Appl.* **3**(6) 064014 URL <https://link.aps.org/doi/10.1103/PhysRevApplied.3.064014>
- [60] Agasti S, Shukla A and Nesladek M 2023 *arXiv preprint arXiv:2301.09974* URL <https://arxiv.org/abs/2301.09974>
- [61] Wang J Q, Yang Y H, Li M, Hu X X, Surya J B, Xu X B, Dong C H, Guo G C, Tang H X and Zou C L 2021 *Phys. Rev. Lett.* **126**(13) 133601 URL <https://link.aps.org/doi/10.1103/PhysRevLett.126.133601>
- [62] Huang R, Miranowicz A, Liao J Q, Nori F and Jing H 2018 *Phys. Rev. Lett.* **121**(15) 153601 URL <https://link.aps.org/doi/10.1103/PhysRevLett.121.153601>
- [63] Bruch A W, Liu X, Guo X, Surya J B, Gong Z, Zhang L, Wang J, Yan J and Tang H X 2018 *Appl. Phys. Lett.* **113** URL <https://pubs.aip.org/aip/apl/article/113/13/131102/35479>
- [64] Zhang M, Buscaino B, Wang C, Shams-Ansari A, Reimer C, Zhu R, Kahn J M and Lončar M 2019 *Nature* **568** 373–377 URL <https://www.nature.com/articles/s41586-019-1008-7>
- [65] Chen J Y, Li Z, Ma Z, Tang C, Fan H, Sua Y M and Huang Y P 2021 *Phys. Rev. Appl.* **16**(6) 064004 URL <https://link.aps.org/doi/10.1103/PhysRevApplied.16.064004>
- [66] Liu X, Bruch A W, Lu J, Gong Z, Surya J B, Zhang L, Wang J, Yan J and Tang H X 2019 *Nat. Commun.* **10** 2971 URL <https://www.nature.com/articles/s41467-019-11034-x>
- [67] Liu X, Sun C, Xiong B, Wang L, Wang J, Han Y, Hao Z, Li H, Luo Y, Yan J *et al.* 2017 *Optica* **4** 893–896 URL <https://opg.optica.org/optica/fulltext.cfm?uri=optica-4-8-893&id=370184>
- [68] McNab S J, Moll N and Vlasov Y A 2003 *Opt. Express* **11** 2927–2939 URL <https://opg.optica.org/oe/fulltext.cfm?uri=oe-11-22-2927&id=77823>
- [69] Vlasov Y A and McNab S J 2004 *Opt. Express* **12** 1622–1631 URL <https://opg.optica.org/oe/fulltext.cfm?uri=oe-12-8-1622&id=79595>
- [70] Bogaerts W, De Heyn P, Van Vaerenbergh T, De Vos K, Kumar Selvaraja S, Claes T, Dumon P, Bienstman P, Van Thourhout D and Baets R 2012 *Laser Photonics Rev.* **6** 47–73 URL <https://onlinelibrary.wiley.com/doi/abs/10.1002/lpor.201100017>
- [71] Zhao Y, Aritomi N, Capocasa E, Leonardi M, Eisenmann M and *et al* 2020 *Phys. Rev. Lett.* **124**(17) 171101 URL <https://link.aps.org/doi/10.1103/PhysRevLett.124.171101>
- [72] Yap M J, Cripe J, Mansell G L, McRae T G, Ward R L, Slagmolen B J, Heu P, Follman D, Cole

- G D, Corbitt T *et al.* 2020 *Nat. Photonics* **14** 19–23 URL <https://www.nature.com/articles/s41566-019-0527-y>
- [73] Dayan B, Pe'er A, Friesem A A and Silberberg Y 2004 *Phys. Rev. Lett.* **93**(2) 023005 URL <https://link.aps.org/doi/10.1103/PhysRevLett.93.023005>
- [74] Gu W j, Li G x and Yang Y p 2013 *Phys. Rev. A* **88**(1) 013835 URL <https://link.aps.org/doi/10.1103/PhysRevA.88.013835>
- [75] Sánchez Muñoz C and Jaksch D 2021 *Phys. Rev. Lett.* **127**(18) 183603 URL <https://link.aps.org/doi/10.1103/PhysRevLett.127.183603>
- [76] Zhang J, Peng B, Özdemir i m c K, Liu Y x, Jing H, Lü X y, Liu Y l, Yang L and Nori F 2015 *Phys. Rev. B* **92**(11) 115407 URL <https://link.aps.org/doi/10.1103/PhysRevB.92.115407>
- [77] Yao X Y, Ali H, Li F L and Li P B 2022 *Phys. Rev. Appl.* **17**(5) 054004 URL <https://link.aps.org/doi/10.1103/PhysRevApplied.17.054004>
- [78] Grudinin I S, Lee H, Painter O and Vahala K J 2010 *Phys. Rev. Lett.* **104**(8) 083901 URL <https://link.aps.org/doi/10.1103/PhysRevLett.104.083901>
- [79] Jing H, Özdemir S K, Lü X Y, Zhang J, Yang L and Nori F 2014 *Phys. Rev. Lett.* **113**(5) 053604 URL <https://link.aps.org/doi/10.1103/PhysRevLett.113.053604>
- [80] Meystre P 2017 *Physics Today* **70**(58) URL <https://pubs.aip.org/physicstoday/article/70/2/58/660204/Cavity-Optomechanics-Nano-and-Micromechanical>